EMAS
Engineering Modelling, Analysis & Simulation
THE NAFEMS JOURNAL

NAFEMS
Vol. 4, Issue 1, 2027

Shape design of a morphing elevator to enhance aircraft low speed efficiency of a regional aircraft

Diego Giuseppe Romano[a,1], Mauro Minervino[a], Domenico Quagliarella[a]

[a]C.I.R.A. SCpA – Italian Aerospace Research Centre, Via Maiorise SNC, Capua (CE) 81043, Italy

Abstract

Control surface aerodynamics plays a crucial role in aircraft performance, both in cruise and low speed conditions, where fuel consumption and stability are most critical. This study presents an aerodynamic shape design based on numerical optimization applied to a future green aircraft elevator, to reduce its drag, maintaining required stability and control authority during the low-speed phases. A numerical aerodynamic optimization based on the application of Covariance Matrix Adaptation Evolution Strategy (CMA-ES) to Computational Fluid Dynamics (CFD) has been performed to identify aerodynamic improvements of the baseline configuration. The methodology integrated parametric shape modifications, by means of Radial Basis Functions (RBFs), assuring a smooth elevator's deflection maximizing aerofoil's lift capabilities, improving or keeping baseline's efficiency. The optimization process was executed under representative low speed conditions (Mach number equal to 0.23, sea level altitude, International Standard Atmosphere (ISA) with temperature difference deviation null – $\Delta T = 0°\mathrm{K}$ –), so results are directly applicable to operational flight regimes. Results demonstrate that the optimized elevator can improve aerofoil lift (up to above 9%), reducing drag (up to above 7%), contributing to improve fuel efficiency (up to 10% aerodynamic efficiency improvement), reducing environmental impact. The study highlights the importance of tailoring control surface geometry also for low-speed efficiency, an aspect often overlooked in conventional design practices. This work underscores the potential of aircraft design advanced optimization techniques, offering a pathway toward more sustainable and cost-effective operations. The methodology presented can be extended to other control surfaces and flight regimes, reinforcing the role of aerodynamic optimization in modern aircraft development. The activities here reported have been carried out within the EU-funded research project HERFUSE (Hybrid-Electric Regional FUSelage & Empennages), aimed to develop advanced designs for the fuselage and empennages of Hybrid-Electric Regional (HER) aircraft.

Keywords

aerodynamics, aircraft, design, elevator, greening, low-speed, morphing, optimization, radial basis functions.

© (2026) The Authors. Published by NAFEMS Ltd.
This work is licensed under a Creative Commons Attribution-NonCommercial-NoDerivatives 4.0 International License.
Peer-review under responsibility of the NAFEMS EMAS Editorial Team.



1 Introduction

International efforts to address climate change emerged from the growing scientific evidence that human activities, particularly the combustion of fossil fuels, were increasing greenhouse gas concentrations and altering the Earth's climate system. This awareness led to the adoption of the United Nations Framework Convention on Climate Change (UNFCCC) at the 1992 Rio Earth Summit [1], establishing the first global framework for climate action. However, the absence of binding emission reduction targets highlighted the need for a permanent forum to monitor progress and strengthen commitments, leading to the creation of the annual Conference of the Parties (COP) [2].

[1]Corresponding author.
E-mail address: d.romano@cira.it (D. Romano)
https://doi.org/10.59972/91k9rwmr

A major milestone was achieved at COP3 in 1997 with the adoption of the Kyoto Protocol [3], the first legally binding agreement requiring industrialized countries to reduce greenhouse gas emissions. Given its limited scope, negotiations continued toward a more inclusive framework, culminating in the Paris Agreement at COP21 in 2015 [4]. Under this framework, countries commit to Nationally Determined Contributions (NDCs), with the goal of keeping the increase in global average temperature well below 2°C above pre-industrial levels while pursuing efforts to limit it to 1.5°C.

As attention increasingly focused on sectors with rapidly growing emissions, international aviation became a key area of action. The International Civil Aviation Organization (ICAO) adopted the Carbon Offsetting and Reduction Scheme for International Aviation (CORSIA) in 2016 [5], the first global market-based mechanism covering an entire sector, aimed at stabilizing net CO_2 emissions from international aviation at 2020 levels. Building on this approach, ICAO endorsed a Long-Term Aspirational Goal (LTAG) in 2022 [6] to achieve net-zero carbon emissions by 2050 through a combination of aircraft efficiency improvements, operational measures, Sustainable Aviation Fuels (SAF), and market-based mechanisms.

In parallel, the European Union aligned its aviation policies with the global framework by supporting ICAO initiatives, including CORSIA, and integrating their principles into the EU Emissions Trading System (EU ETS) [7], which requires airlines to monitor, report, and reduce emissions. These measures contribute to the EU's broader objective of climate neutrality under the European Green Deal [8].

To further accelerate this transition, the EU established the Clean Aviation Joint Undertaking (CAJU) [9] under the Horizon Europe programme. Through the Clean Aviation Programme, CAJU promotes collaboration among industry, policymakers, and research institutions to develop the technologies needed for climate-neutral aviation by 2050, focusing on three main areas: hybrid-electric and hydrogen-powered aircraft, ultra-efficient aircraft designs, and the integration of Sustainable Aviation Fuels.

In the frame of Clean Aviation, the research project HERFUSE has been launched to develop advanced designs for the fuselage and empennages of HER aircraft.

The present paper presents the design activities carried out by the Italian Aerospace Research Centre (CIRA) within HERFUSE Project, aimed at the development of an innovative morphing elevator for a future greener regional aircraft to improve airplane performance and reduce its environmental impact under realistic flight conditions, representing the low speed – i.e. take-off and landing – phases.

Currently, in fact, morphing technologies have been widely studied for application to wings and high lift devices, while less effort has been focused on their application to tailplanes. However, in conventional configurations, the elevator has to generate an aerodynamic force balancing wing's pitching moment. Thus, a trim drag contribution is introduced to overall aircraft drag, reducing aircraft efficiency, thus increasing fuel consumption and pollutant emissions. Allowing the elevator to adapt its geometry during the several flight phases, trim drag penalty can be minimized. As a consequence, control surface deflections can be reduced, and overall aerodynamic efficiency can be increased, leading to fuel consumption (i.e. pollution) reduction.

The work reported here aims to develop an aero optimization framework, based on the use of Covariance Matrix Adaptation Evolution Strategy (CMA-ES), a stochastic evolutionary optimization algorithm belonging to the family of Evolution Strategies (ES), specifically designed for continuous black-box optimization problems, and Radial Basis Functions (RBFs), a function approximation and interpolation technique based on radially symmetric basis functions, specifically designed to model complex nonlinear relationships from scattered multidimensional data, to evaluates elevator's performance in a typical range of tailplane angles of attack in low-speed conditions. The design goals are to:

- Enhance aerodynamic efficiency, thanks to the alignment of transverse load distribution of the elevator with cruise requirements.
- Reduce trim drag by tailoring the shape of the elevator to minimize un-required axial force (drag) in steady flight.
- Support environmental targets set by ACARE and the European Union, thanks to the contribution to reductions in fuel burn, CO_2 emissions, and noise.

The procedure developed can be applied to design other aircraft control surfaces and consider other flight phases, assuring the its versatility.

The paper is structured as follows: after a brief discussion about the state of the art of morphing technology applied to aviation sector, the methodology developed and applied to design the

aerodynamic shape of the elevator is presented. Subsequently, the discussion focuses on the description of the optimization problem, its set-up and the results obtained. Finally, the conclusions are summarized and next steps to be taken are suggested.

- Background and state of the art: this section briefly focuses on the state of the art of morphing technology applied to aviation sector.
- Methodology: this section presents the methodology developed and applied to design the aerodynamic shape of the elevator.
- Optimization set-up: this section describes the optimization problem and its set-up.
- Results: this section summarizes the outcomes of the analyses performed.
- Conclusions and way forward: this section provides the conclusion of the work carried out and the next steps to be taken.

2 Materials and Methods

This section is aimed at the provision of background and state of the art (§2.1), of the methodology developed (§2.2), and of the optimization problem solved (§2.3).

2.1 Background and state of the art

This section is devoted to providing a brief description of the background and state of the art (SoA) of the morphing technology in aviation sector.

2.1.1 Literature review

Morphing structures have gained increasing attention and interest in the aeronautical community as a means to increase aircraft aerodynamic efficiency, thus, to reduce overall environmental impact.

Morphing technologies are based on the use of advanced actuation, compliant structures, and smart materials to actively modify the shape of a body. Research by [10] explored coordinated control strategies integrating structural deformation with flight dynamics through piezoelectric patch actuation. According to [11], advances in shape memory alloys have enabled lightweight, reliable morphing mechanisms. These developments provide the technological foundation for applying morphing concepts to elevators, where adaptive geometry can contribute to noise reduction, improvements of stability margins and trim drag reduction [12].

A comprehensive review of the application of morphing structures in aircraft is available in [13][10]. According to the Authors, morphing concepts can be categorized into three different types: planform alteration, out of plane deformation, and aerofoil deformation. In the case of planform alteration, the wing changes its overall size or layout (e.g., telescopic span extension or variable-sweep wings), affecting global aerodynamic characteristics such as lift-to-drag ratio and cruise efficiency. A typical example of such typology is the F-14 variable-sweep wing. In the case of out-of-plane transformation, the wing bends or twists without significantly changing its planform. This allows load control and aerodynamic tuning during flight, often replacing or augmenting conventional control surfaces. In the case of aerofoil deformation, the wing modifies its aerofoil shape to adapt it to different flight conditions, improving lift or reducing drag. This class includes many modern morphing devices, such as the one studied in this work.

All the three different typologies can be successfully applied to reduce aircraft drag and noise. A recent survey by [14], emphasize the integration of lightweight, intelligent morphing structures into advanced aircraft design. In particular, it is noted the important role of such innovative structures to reduce energy consumption and improving aerodynamic adaptability of the configurations mounting morphing devices.

It must be noted that up to now the application of morphing technology to wings and flaps has received considerable attention so far, while control surfaces (particularly those on tailplanes) have been explored less extensively. However, recent studies confirm their potential of morphing technology to reduce trim drag, improving aircraft stability. In particular, [15] investigated the unsteady aerodynamic characteristics of morphing tail configurations. According to the Author, adaptive tails can reduce trim drag, while improving aircraft stability, under varying flight conditions. This confirms that morphing elevator can directly contribute to efficiency gains in regional aircraft, where multiple flight regimes must be balanced during the aeroplane operative mission.

As anticipated in the previous sections, the ACARE Flightpath 2050 vision and EU climate policies set ambitious goals for aviation industry targeting a reduction of 75% in CO_2 emissions per passenger kilometre, 90% in NO_X (Nitrogen Oxides), and 65% in perceived noise by 2050. To meet these ambitious goals, the EU launched several research programs such as Clean Sky (2008-2018), Clean Sky 2 (2014-2024) and the currently active Clean Aviation. These programs have funded demonstrators incorporating several innovative technologies, including morphing technologies. In particular, the Morphing Wing Project [16] demonstrated morphing leading edge and trailing edge devices for regional aircraft, and achieved measurable drag and noise reductions, including 6–15% drag reduction, 3–12% fuel savings, and up to a 45% reduction in take-off noise [17], [18]. Similarly, Leonardo's C-27J Flying Testbed validated morphing surfaces and control algorithms, showing the feasibility of integrating adaptive structures into operational platforms [19].

In the past years, the design and optimization of aircraft tailplanes has been deeply studied for conventional aircraft stability and control, because tailplanes are essential for aircraft equilibrium, trimming capability, and overall aerodynamic efficiency. However, these studies were not focused on the application of morphing technology to tailplanes, so the integration of such technology in aircraft design is a cutting edge and emerging research direction.

Under an historical standpoint, researcher have tried to improve stability margins and reduce drag penalties by means of semi empirical sizing methods, numerical investigations, and wind tunnel experiments. In particular, [20] provided comparative guidelines for preliminary tailplane sizing in regional aircraft and [21] reviewed semi empirical approaches for vertical tail design. In addition, some experimental campaigns explored innovative geometries with sweep variations and stall control devices, demonstrating that conventional tailplane design can be improved by means of aerodynamic tailoring [22].

Despite conventional elevators have been deeply investigated over the years, the application of morphing technology to elevators is a very recent development. Up to now, in fact, tailplane studies have mainly assumed rigid geometries, with optimization focused on fixed planform parameters and/or plane incidence angle. Thus, morphing technology introduces a new degree of freedom, because it allows the modification of elevator's shape in flight. This represents a fundamental shift in approach, making it possible to achieve adaptive trimming and efficiency gains that traditional fixed configurations cannot offer. Morphing elevators thus emerge as a genuinely disruptive innovation, marking a significant functional advancement by integrating aerodynamic flexibility with advanced optimization methods like evolutionary algorithms and surrogate modelling. Meanwhile, widely used academic materials — such as the Massachusetts Institute of Technology (MIT) notes on stability and control [23] — still emphasize the elevator's conventional role in trim and pitch moment balance, without yet addressing morphing technologies. This gap further highlights the originality and innovative nature of the approach introduced in this paper.

2.1.2 Aerodynamic design through numerical optimization

The growing demand for improved fuel efficiency, emissions reduction, and enhanced performance in modern aircraft has strongly stimulated research in numerical aerodynamic optimization. This design approach relies on computational tools to refine aerodynamic shapes and configurations, allowing designers to investigate much broader design spaces than those typically accessible through experimental testing alone or classical design procedures. In this framework, aerodynamic optimization combines Computational Fluid Dynamics (CFD) with advanced optimization algorithms to identify solutions that satisfy specific objectives while respecting imposed constraints, based on the overall requirements of the aircraft configuration under study.

Multidisciplinary Design Optimization (MDO) is one of the most influential paradigms in optimization, integrating multiple disciplines such as aerodynamics, control system, propulsion and/or structures. By coupling these areas, MDO enables engineers to assess trade-offs across different disciplines, ensuring that gains in aerodynamic performance do not negatively impact other domains. Recent studies emphasize that MDO has become a fundamental component of modern aircraft design, particularly for regional and commercial transport applications, where even small efficiency improvements can lead to substantial reductions in operating costs [24].

Optimization techniques can generally be divided into two main categories: gradient-based methods and evolutionary algorithms. Gradient-based methods are iterative procedures that exploit derivatives of the objective function to locate minima or maxima, progressing in the direction of steepest descent or ascent through incremental updates. Among the most used approaches we can mention the Adaptive Moment Estimation (ADAM), the Gradient Descent, the Momentum method, and the Nesterov

Accelerated Gradient (NAG). These methods are particularly effective when dealing with smooth response surfaces, as they ensure fast convergence when sensitivity information is available. However, their performance may degrade in highly nonlinear or discontinuous design spaces, where they are prone to becoming trapped in local optima [25].

In contrast, evolutionary algorithms offer greater robustness when exploring complex and multimodal design spaces. Techniques such as GAs and the CMA-ES have proven successful in aerodynamic shape optimization, especially when combined with surrogate modelling approaches. In particular, surrogate models based on RBFs provide efficient approximations of CFD results, significantly reducing computational costs while maintaining acceptable accuracy [26].

More recently, mid-fidelity numerical methods have gained increasing attention within the scientific community. These approaches aim to strike a balance between computational efficiency and predictive accuracy, making them especially suitable for tackling challenges associated with emerging aircraft concepts, such as distributed electric propulsion systems and other unconventional configurations. The adoption of reduced-order models and hybrid CFD techniques enables the capture of the dominant aerodynamic phenomena while preserving manageable optimization workflows [27].

Aerodynamic optimization also plays a key role in the design of unconventional aircraft architectures. For instance, it has been successfully applied to box-wing configurations and Boundary Layer Ingestion (BLI) propulsion systems, demonstrating its capability to exploit the interaction between aerodynamics and propulsion. These integrated approaches have led to notable reductions in fuel consumption and emissions [28]. Similarly, numerical aerodynamic optimization has been widely employed in the development of Unmanned Aerial Vehicles (UAVs), enabling the design of tailored wing and fuselage geometries that maximize endurance and manoeuvrability while complying with strict weight limitations [29].

The next frontier in aerodynamic design lies in the development of integrated frameworks that combine CFD, surrogate modelling, and high-performance computing. Such frameworks will make it possible to perform thousands of design evaluations, fostering the exploration of unconventional configurations and enabling the optimization of complete aircraft systems rather than isolated components. Furthermore, the increasing availability of parallel computing resources has accelerated the integration of high-fidelity CFD into optimization loops, thereby reducing reliance on empirical correlations and wind tunnel testing.

In conclusion, numerical aerodynamic optimization has evolved from a tool primarily used for localized shape refinement into a comprehensive, multidisciplinary, system-level design methodology. The integration of advanced optimization algorithms, CFD techniques, and surrogate models now allows engineers and researchers to achieve significant improvements in aerodynamic performance and overall aircraft sustainability. This evolution highlights the pivotal role of computational tools in aeronautics, positioning them not merely as supporting instruments but as fundamental drivers of innovation.

2.2 Methodology

The numerical evaluations have been performed using ADGLIB (the Adaptive Genetic optimization LIBrary) a CIRA in-house optimization tool conceived to apply hybrid optimization algorithms to design problems of industrial interest [30][31] and has also the capability of robust and reliability based optimization [32][33]. ADGLIB allows selection among several optimization algorithms that can be combined in a hybrid fashion. Among these, the Covariance Matrix Adaptation Evolution Strategy (CMA-ES) algorithm [34] was selected for the design problem presented here. The update of elevator geometry is obtained thanks to a dedicated routine developed by CIRA to perform RBFs interpolation [35].

The selected flow solver used to evaluate aerodynamic performance for the designed configurations is an interactive solver based on an integral boundary layer, coupled with a structured Euler solver.

2.2.1 CMA-ES optimization algorithm

The aerodynamic optimization problem considered in this study is characterized by a strong coupling between the aerofoil geometric design variables and the resulting aerodynamic performance. Geometric modifications aimed at reducing drag may simultaneously affect lift, pressure distribution, shock location, and boundary-layer development. Consequently, drag minimization competes with the requirement of maintaining a prescribed minimum lift coefficient, as solutions achieving lower drag at the expense of insufficient lift are not admissible within the considered design constraints. Moreover,

transonic flow phenomena, including shock-wave displacement, viscous effects, boundary-layer transition, and possible flow separation, can introduce strong nonlinearities in the aerodynamic response, such that relatively small geometric variations may lead to significant changes in the aerodynamic coefficients. This results in a complex and potentially multimodal design space. For these reasons, the CMA-ES was adopted as a derivative-free optimization method, providing a robust framework for exploring nonlinear and potentially non-smooth design spaces.

CMA-ES is a stochastic evolutionary optimization algorithm particularly suited to nonlinear, non-convex, and potentially multimodal optimization problems. It employs a population-based approach in which, at each generation, candidate solutions are sampled from a multivariate normal distribution whose parameters are iteratively adapted according to the performance of the evaluated solutions. In particular, the covariance matrix controls the shape and preferential search directions of the distribution, while the global step size, σ, controls its overall scale, thus regulating the extent of the exploration of the design space. The CMA-ES update mechanism is based on the mean vector $\boldsymbol{m}_t$ and the covariance matrix $\boldsymbol{C}_t$ of the sampling distribution. At the start, the algorithm sets the initial mean $\boldsymbol{m}_0$, assigns the covariance matrix to the identity matrix $\boldsymbol{C}_0 = I$, defines the global scale factor σ_0 (i.e. the standard deviation of the initial multivariate Gaussian that determines the amplitude of the mutation step), and initializes additional internal variables such as the evolution paths.

A new population of λ candidate solutions is then generated by sampling from the current multivariate normal distribution:

$$\boldsymbol{x}_k = \boldsymbol{m}_t + \sigma_t \boldsymbol{C}_t^{1/2} \boldsymbol{z}_k \quad \text{for } k = 1, \dots, \lambda, \tag{1}$$

where $\boldsymbol{z}_k \sim \mathcal{N}(\boldsymbol{0}, \boldsymbol{I})$ represents a standard normal random vector. Each sampled candidate is evaluated using the objective function. The best μ individuals are selected according to their fitness values and used to compute the updated mean:

$$\boldsymbol{m}_{t+1} = \sum_{i=1}^{\mu} w_i \, \boldsymbol{x}_{i:\lambda} \tag{2}$$

where $\boldsymbol{x}_{i:\lambda}$ denotes the i-th best individual and w_i is its associated weight. The algorithm proceeds by updating the evolution paths $\boldsymbol{p}_c$ and $\boldsymbol{p}_\sigma$, which control the adaptation of the covariance matrix and the step size, respectively. Subsequently, the covariance matrix $\boldsymbol{C}_t$ is adjusted:

$$\boldsymbol{C}_{t+1} = \left(1 - c_1 - c_\mu\right)\boldsymbol{C}_t + c_1 \boldsymbol{p}_c \boldsymbol{p}_c^T + c_\mu \sum_{i=1}^{\mu} w_i \, \boldsymbol{z}_{i:\lambda} \boldsymbol{z}_{i:\lambda}^T \tag{3}$$

In the final step, the step size σ_t is modified based on the evolution path p_σ.

Through the adaptation of the covariance matrix, CMA-ES can capture the structure of the objective function, allowing it to guide the search efficiently by progressively reshaping the sampling distribution across generations.

2.2.2 Radial Basis Functions for geometry update

RBFs are a class of mathematical functions defined as a function of the distance between a point and a given centre, which makes them intrinsically radially symmetric. They are commonly used for interpolation and surrogate modelling, as they can effectively approximate complex, high-dimensional relationships from scattered datasets without the need for a structured computational grid [35]. In practice, RBFs are employed to reconstruct scalar field values at arbitrary locations in space based on known values at a set of discrete source points. For multidimensional problems, this interpolation process can be applied independently to each scalar quantity of interest. By selecting different kernel types — such as Gaussian, multiquadric, or inverse multiquadric — RBFs provide flexibility in tuning smoothness and locality, making them particularly suitable for applications in numerical analysis, mesh-free techniques, and optimization methods [36], [37].

In the present work, second-order polyharmonic spline RBFs are adopted to interpolate the displacement field from a selected set of control points — used to define the deformation of the aerofoil trailing edge — to the entire set of aerofoil geometry points. This choice is motivated by the fact that the CFD mesh is constructed from a discrete geometric representation in which the aerofoil shape is defined by a finite set of coordinate points. Since the deformation is intended to affect only the elevator portion, the source points are defined to include all geometry points located upstream of the movable segment ($x/c < \tilde{x}_{elev}$), where a zero-displacement condition is imposed.

To control the deformation of the elevator, three additional source points are introduced: the two trailing-edge points (located at $x/c = 1$, corresponding to the upper and lower endpoints of the finite-thickness trailing edge), and an intermediate control point positioned along the elevator chord line at $x/c = \tilde{x}_{elev} + (1 - \tilde{x}_{elev})/eq_{div}$, where its exact location is determined by the parameter eq_{div} (see Figure 1).

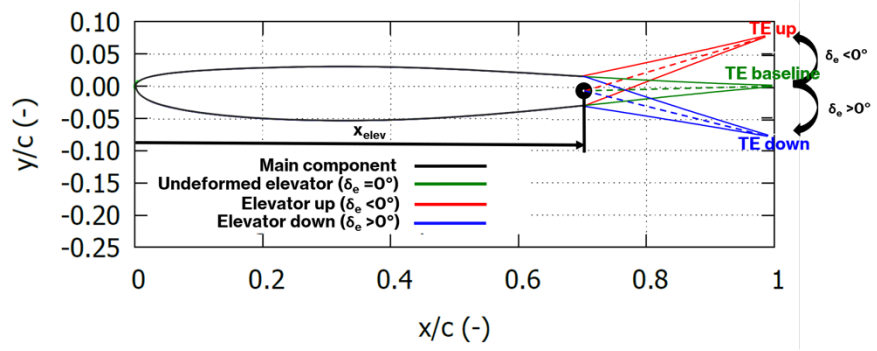


Figure 1. Example of elevator deflection.

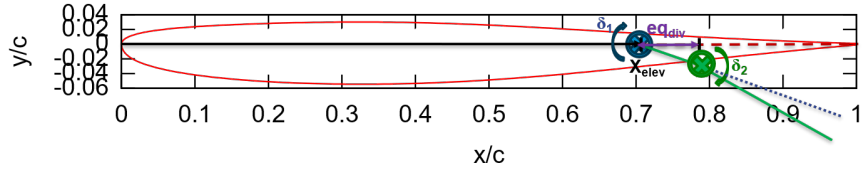


Figure 2. Design variables.

The prescribed displacements at these three points are obtained by applying rigid-body rotations about the point $(\tilde{x}_{elev}, 0)$. Specifically, the trailing-edge points undergo a rotation of δ_{te}degrees, while the intermediate point rotates by $\delta_i$degrees, with positive angles corresponding to downward deflections (see Figure 2).

The continuous displacement field is then obtained by solving the RBF interpolation problem using the defined set of source points and their associated displacement values. This field is subsequently evaluated at all aerofoil geometry points to propagate the deformation consistently. By construction, the RBF solution enforces zero displacement at all points where $x/c < \tilde{x}_{elev}$. As a result, the deformation is smoothly applied only to the elevator region, from $x/c = \tilde{x}_{elev}$ to $x/c = 1$, while also preserving the original trailing-edge thickness (Figure 3).

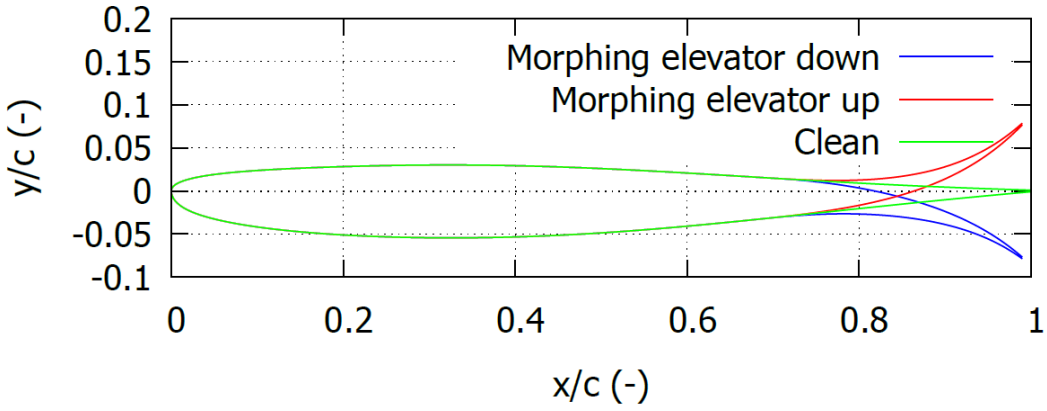


Figure 3. Possible morphed shapes.

2.3 Optimization set-up

This section describes the optimization problem analysed, providing the problem definition, the definition of the conditions and optimization goals, and the parameterization used.

2.3.1 Optimization Problem Definition

The present work addresses the optimization of the aerodynamic performance of a two-dimensional (2D) aerofoil section representative of a horizontal tailplane. In particular, the selected geometry corresponds to the Mean Aerodynamic Chord (MAC) section of the lifting surface. The objective is the maximization of aerodynamic efficiency, expressed in terms of the lift-to-drag ratio:

$$E = \frac{C_l}{C_d}, \tag{4}$$

under steady low-speed conditions.

The reference flight condition adopted throughout the analysis is defined as follows:

- Mach number: $M = 0.23$,
- Altitude: $h = 0$ft,
- Atmospheric model: ISA with $\Delta T = 0°$K deviation.

To guarantee a fair comparison between conventional and innovative configurations, constraints are imposed on the lift coefficient. Specifically, each candidate solution must ensure a lift coefficient magnitude at least equal to that of the baseline configuration. This requirement is applied in absolute value, accounting for the fact that the aerofoil may operate under both positive and negative lift conditions depending on the tailplane trim requirements.

The baseline configuration consists of a reference aerofoil equipped with a conventional elevator, modelled as a rigid control surface hinged at a fixed point located at $(\tilde{x}_{elev}, 0)$. The elevator undergoes a pure rotational motion about this hinge.

2.3.2 Baseline Geometry and Operating Conditions

The elevator geometry is defined according to the following assumptions:

- Elevator chord equal to 30% of the reference aerofoil chord,
- Maximum deflection range: $\delta_e = \pm 15°$,
- Hinge location positioned at half of the rear spar thickness.

Figure 1 illustrates the baseline aerofoil geometry for the extreme deflection cases, namely $\delta_e = +15°$(downward deflection, blue line) and $\delta_e = -15°$(upward deflection, red line).

A total of six representative design points is selected to capture the relevant operating envelope of the tailplane. These points are defined as follows:

- Three conditions correspond to a downward elevator deflection of $+15°$, combined with incidence angles of $-3.00°$, $0.00°$, and $3.00°$,
- Three additional conditions correspond to an upward deflection of $-15°$, with incidence angles of $-3.00°$, $0.00°$, and $3.00°$.

For each of these operating points, the aerodynamic performance of the baseline configuration is evaluated, and the corresponding lift coefficient is recorded. These values are subsequently enforced as constraints for all optimized configurations at the same operating conditions.

2.3.3 Objective Function Formulation

The constrained optimization problem is formulated by embedding the lift constraints within the objective function through the use of quadratic penalty terms. The resulting objective function can be expressed as:

$$J = \sum_{i=1}^{6} C_{d,i} + \sum_{i=1}^{6} \Pi_i, \tag{5}$$

where $C_{d,i}$ is the drag coefficient associated with the i-th design point, and $\Pi_i$represents the penalty contribution arising from any violation of the corresponding lift constraint.

This formulation allows the simultaneous consideration of all operating conditions, driving the optimization towards solutions that provide improved overall performance rather than optimality at a single design point.

2.3.4 Morphing Elevator Parameterization

The innovative configurations investigated in this study are based on the concept of a morphing elevator, whose shape is no longer constrained to rigid rotation. Instead, the geometry is parameterized through four independent design variables:

- $\tilde{x}_{elev}$: non-dimensional hinge location, varying in the range [0.7, 0.95],
- δ_{te}: prescribed rotation at the trailing edge, within $[-15°, +15°]$,
- eq_{div}: non-dimensional abscissa of a secondary control point, ranging from 1.05 to 10,
- δ_i: rotation associated with the secondary control point, within $[-15°, +15°]$.

As illustrated in Figure 2, the morphing deformation is governed by two control points: the first (highlighted in red), defined by x_{elev}, and the second (highlighted in blue), defined by eq_{div}. The rotations δ_{te} and δ_i are applied about these respective points, enabling a flexible redistribution of curvature along the control surface. Thus, a total of 4 design variables is used to morph the elevator: hinge location (x_{elev}), the location of a secondary control point managed by a scalar value (eq_{div}), the rotation of trailing edge (δ_{te}) and the rotation around the second control point (δ_i).

The resulting morphing shapes are generated using Radial Basis Functions (RBFs), which ensure smooth and continuous geometric transformations. Representative examples of such configurations are reported in Figure 3.

2.3.5 CFD Flow Solver

The CFD software employed for the aerodynamic analyses is an integrated computational framework developed for both the analysis and design of single- and multi-element aerofoils operating in subsonic and transonic flow regimes. The tool encompasses the entire CFD workflow, including mesh generation based on the input geometry and an initial potential-flow solution, flow-field computation, and post-processing capabilities for result visualization.

The methodology is specifically intended for high-Reynolds-number applications, where the boundary-layer approximation remains valid. The external flow domain is assumed to be inviscid and is governed by the two-dimensional Euler equations, whereas the near-wall region, where viscous effects become significant, is represented through integral boundary-layer formulations. The interaction between these two regions is achieved through an Interactive Boundary Layer (IBL) approach, which ensures consistency between the pressure field predicted by the inviscid solver and the displacement effects generated by the viscous boundary layer. This coupling strategy is particularly important for aerofoils operating in transonic conditions, where shock-wave interactions, boundary-layer development, and local flow separation strongly influence aerodynamic performance. The code is therefore capable of modelling weak shock-boundary-layer interactions as well as limited separated-flow regions.

At the core of the flow solver lies a nonlinear Newton-based algorithm that simultaneously couples the global simulation variables, such as angle of attack, prescribed lift coefficient, and Mach number, thereby providing a robust and efficient solution procedure.

In addition to direct aerodynamic analyses, the same computational framework can be applied to inverse design problems. In this configuration, the user specifies a target pressure distribution, and the solver iteratively modifies the aerofoil geometry until the desired aerodynamic characteristics are achieved.

From a mathematical standpoint, the solver combines the Euler equations, which describe the conservation of mass, momentum, and energy in a compressible inviscid flow, with integral boundary-layer equations that account for viscous phenomena. This formulation significantly reduces the computational cost compared with full Navier-Stokes simulations while maintaining a satisfactory level of physical fidelity and modelling flexibility. The solver can model both natural and forced boundary-layer transition, as well as shock-wave interaction effects that are characteristic of transonic flows. Through an iterative viscous-inviscid coupling procedure, the pressure distribution and boundary-layer displacement thickness are continuously updated until convergence is achieved, enabling the accurate prediction of phenomena such as boundary-layer growth, displacement effects, and shock formation.

The software can be applied to both single-element and multi-element aerofoils, making it particularly suitable for the analysis of configurations incorporating movable aerodynamic surfaces, such as flaps, slats, and elevators.

2.3.6 Scope of the Optimization

The optimization procedure aims to assess the potential benefits of morphing technology in enhancing the aerodynamic efficiency of the tailplane section across the entire set of operating conditions. Unlike the conventional configuration, which relies on rigid-body rotation, the morphing approach allows for tailored shape adaptation at each design point.

Consequently, the optimization process generally yields six distinct optimal geometries, each associated with a specific combination of incidence angle and control deflection. This highlights the intrinsic capability of morphing systems to provide condition-dependent performance improvements, potentially leading to significant gains in overall aircraft efficiency.

3 Results and Discussion

In this section, the results of the aero-design are reported. In particular, as mentioned in the previous sections, six different design points have been analysed, 3 with a positive elevator deflection (elevator down) and three with a negative deflection (elevator up).

Elevator morphed designs were obtained by applying the procedure summarized in Section 2.3.4.

The optimization was carried out using the CMA-ES algorithm with an initial global scale factor $\sigma_0 = 0.05$, a population size of 12 elements, and a maximum number of evaluations set at 3000. The best configuration obtained with this first optimization run was then used as the baseline for a new iteration of the CMA-ES algorithm that was set-up using the same parameters.

Figure 4 shows the convergence history of the optimization loop, requiring less than 4000 evaluations to converge.

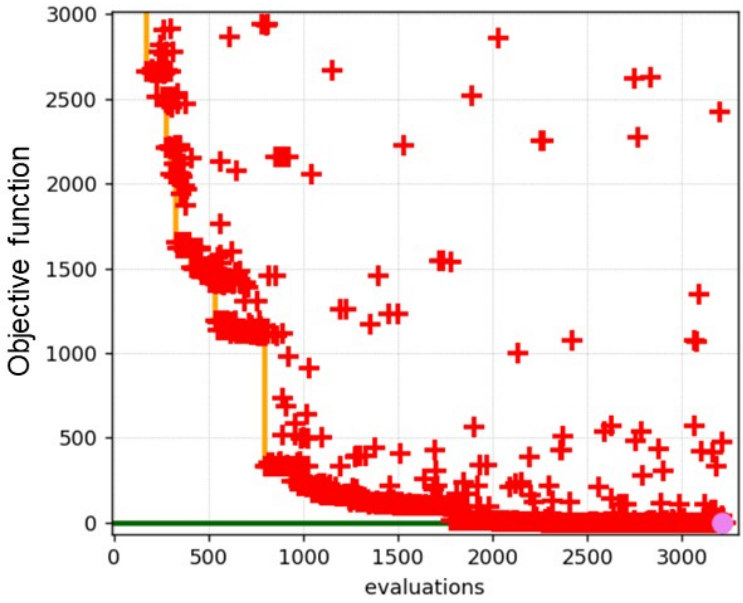


Figure 4. Convergence history.

Figure 5 to Figure 7 show the pressure coefficient distributions around the baseline (red line) and best (green line) aerofoils. It is possible to observe that the elevator morphing sensibly affects the rear part of the pressure coefficient (C_p) distribution, reducing and smoothing the secondary peak.

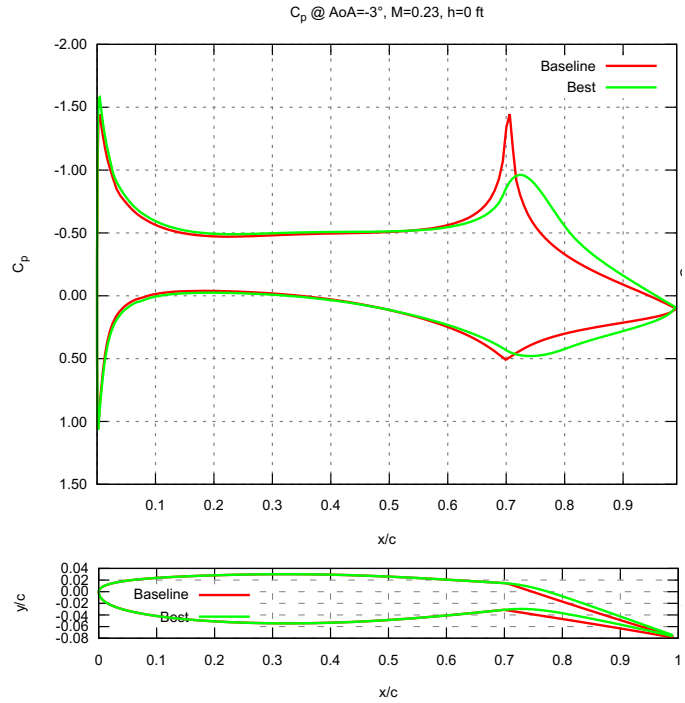


Figure 5. Pressure distributions (up) and aerofoils (bottom) comparisons for the optimization at AoA=-3° and positive elevator deflections (elevator down): baseline (red) vs best (green).

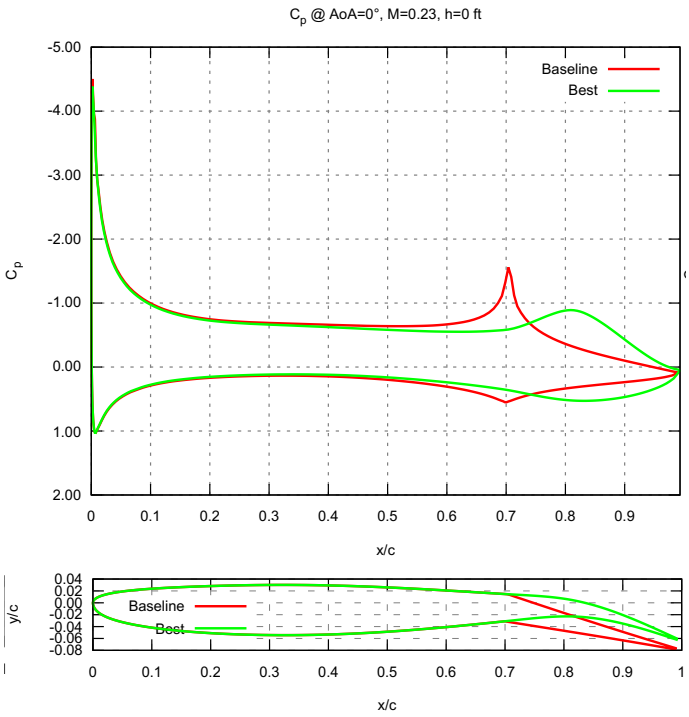


Figure 6. Pressure distributions (up) and aerofoils (bottom) comparisons for the optimization at AoA=0° and positive elevator deflections (elevator down): baseline (red) vs best (green).

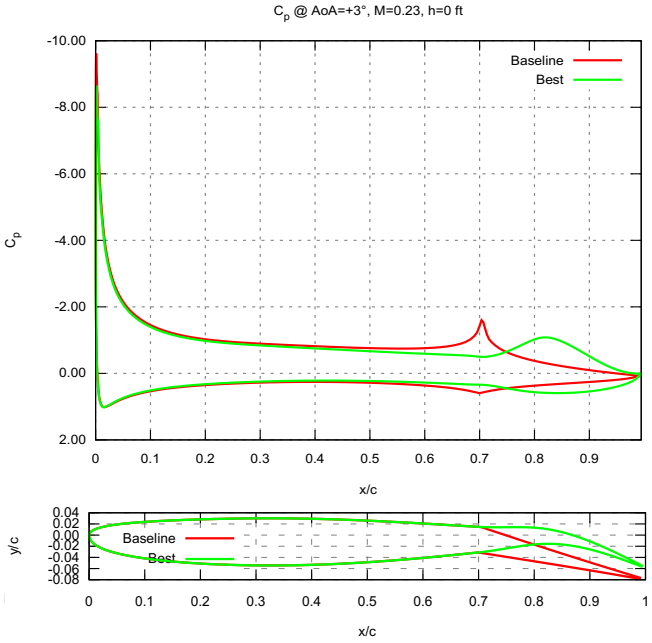


Figure 7. Pressure distributions (up) and aerofoils (bottom) comparisons for the optimization at AoA=+3° and positive elevator deflections (elevator down): baseline (red) vs best (green).

A similar trend can be observed from Figure 8 to Figure 10, referring to the baseline (red) and best (green) designs for a negative elevator deflection (elevator up).

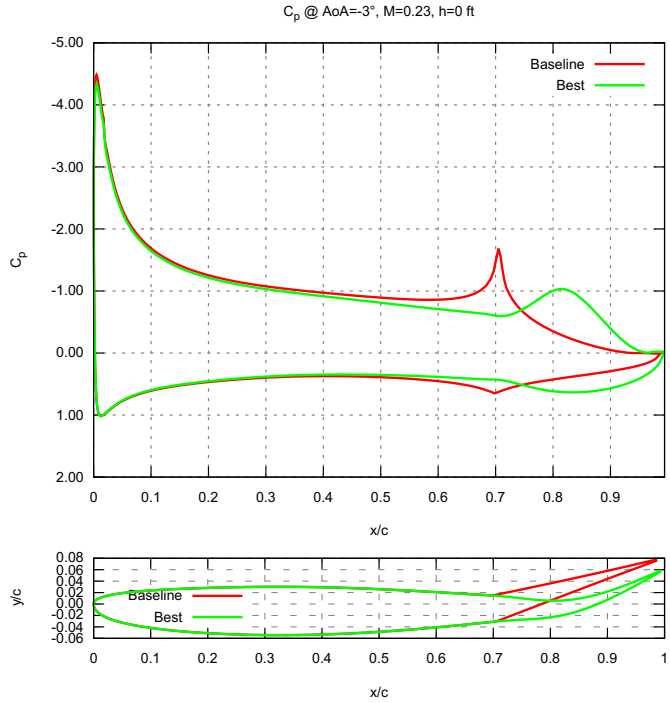


Figure 8. Pressure distributions (up) and aerofoils (bottom) comparisons for the optimization at AoA=-3° and negative elevator deflections (elevator up): baseline (red) vs best (green).

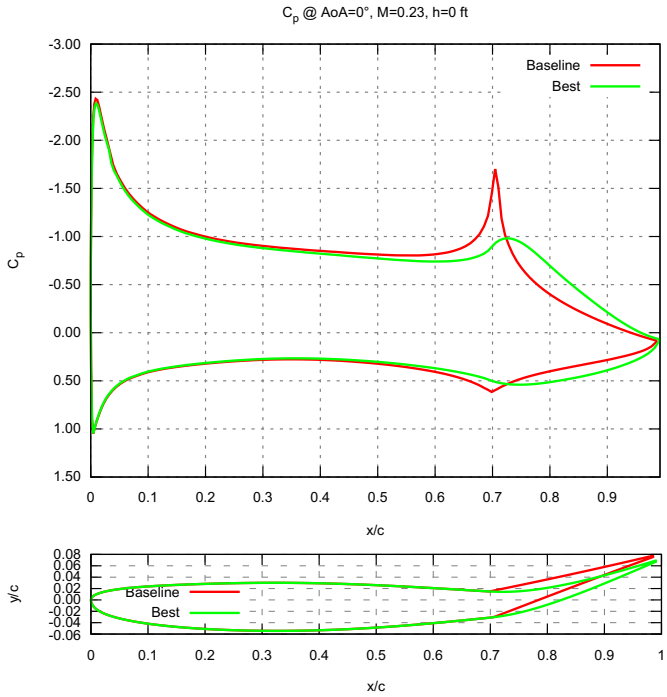


Figure 9. Pressure distributions (up) and aerofoils (bottom) comparisons for the optimization at AoA=0° and negative elevator deflections (elevator up): baseline (red) vs best (green).

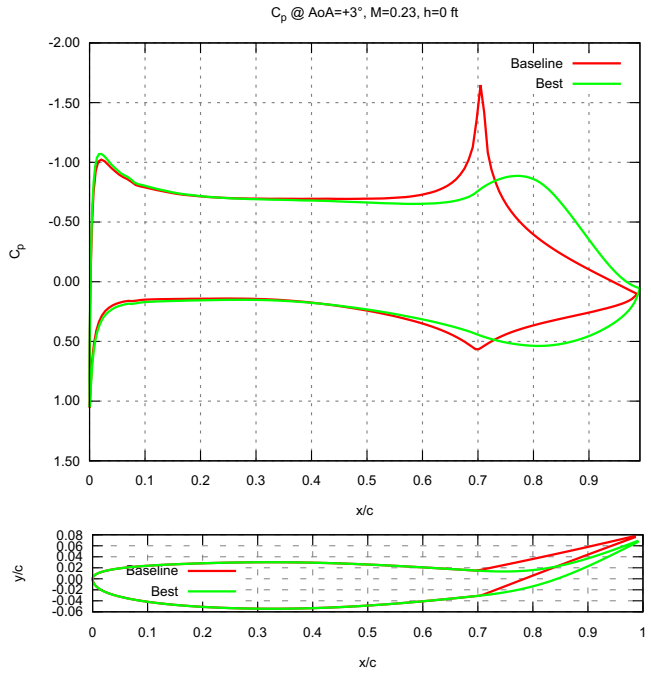


Figure 10. Pressure distributions (up) and aerofoils (bottom) comparisons for the optimization at AoA=+3° and negative elevator deflections (elevator up): baseline (red) vs best (green).

Figure 11 to Figure 14 show the aerofoil's lift coefficient and its efficiency of the morphed elevator (green line) and of the baseline (red line) configuration, as well as the lift coefficient improvements of the morphed elevator for, respectively, elevator down and up position.

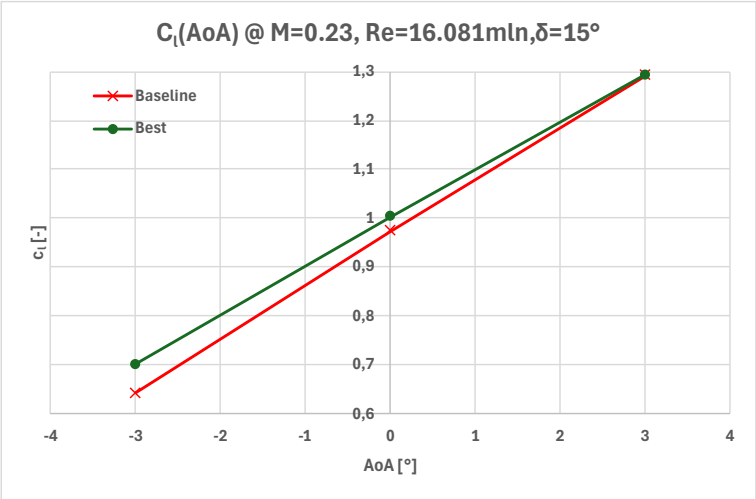


Figure 11. Lift coefficient comparison for the three test cases (red: baseline, green: best) for elevator down.

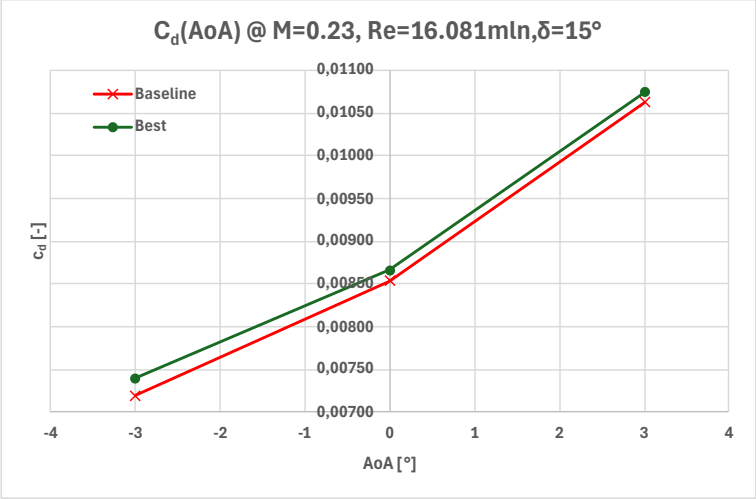


Figure 12. Drag coefficient comparison for the three test cases (red: baseline, green: best) for elevator down.

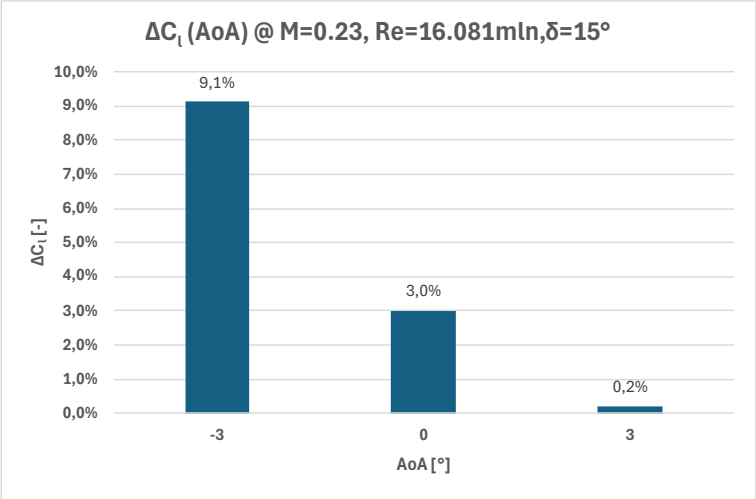


Figure 13. Efficiency comparison for the three test cases (red: baseline, green: best) for elevator down.

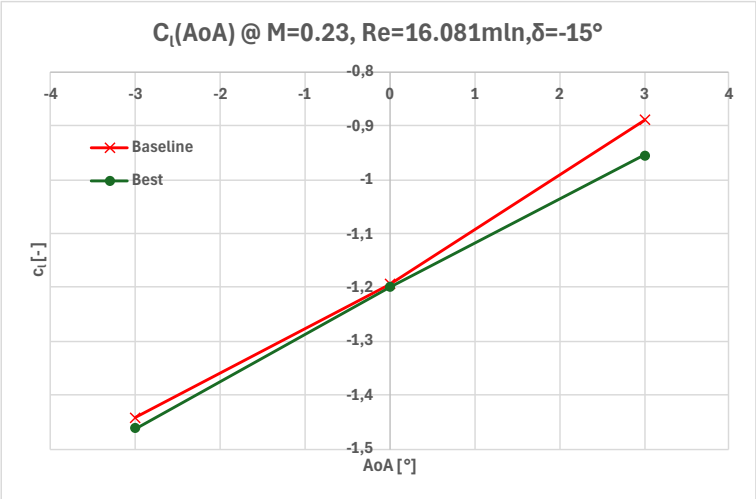


Figure 14. Lift coefficient comparison for the three test cases (red: baseline, green: best) for elevator up.

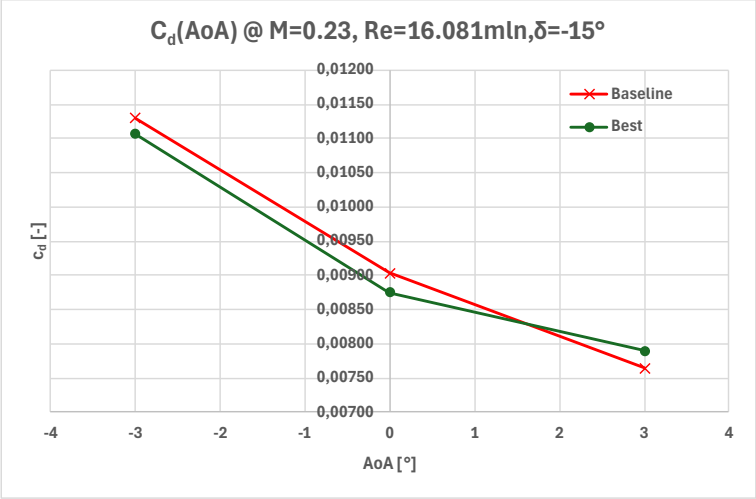


Figure 15. Drag coefficient comparison for the three test cases (red: baseline, green: best) for elevator up.

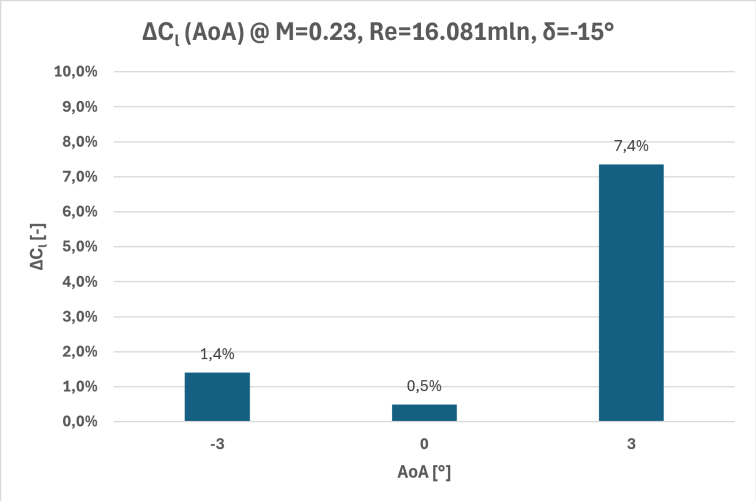


Figure 16. Efficiency comparison for the three test cases (red: baseline, green: best) for elevator up.

It is possible to notice that the morphed elevator guarantees a sensible improvement (above 9%) in the maximum lift coefficient, having in the meantime a positive effect on its efficiency, which is improved for 5 out of 6 design points.

4 Conclusions

This paper has presented a methodology for the design of an advanced morphing elevator for green aircraft applications, highlighting the aerodynamic benefits that can be achieved through an optimized configuration. Starting from a conventional hinged elevator with a cusp-shaped surface, the reference geometry was improved through an aerodynamic optimization process aimed at maximizing the aerofoil maximum lift coefficient under low-speed conditions (M = 0.23, h = 0 ft, ISA atmosphere), while maintaining or enhancing aerofoil efficiency over a prescribed range of elevator deflections (±15°) and angles of attack.

To account for the most demanding operational scenarios, six critical design conditions were selected, resulting in six corresponding optimized aerofoil configurations. The optimization activity was carried out using an in-house numerical framework developed by CIRA, in which the CMA-ES algorithm was adopted to drive the geometric updates. The morphing of the elevator profile was performed through Radial Basis Functions (RBFs), enabling the generation of a smooth and continuous surface capable of improving aerofoil performance, particularly in cruise conditions.

The obtained results demonstrate that the introduction of a smooth morphing elevator can increase the aerodynamic efficiency of the horizontal tail plane by up to approximately 10%. This improvement is mainly associated with the reduction of flow separation on the suction side of the aerofoil, caused by the attenuation of the secondary pressure peak on the upper surface. In particular, the comparison between the pressure coefficient distributions of the baseline and morphing configurations shows that the smooth elevator has a limited impact on the leading-edge expansion, while significantly reducing the rear expansion peak generated at the elevator hinge.

The methodology developed and applied in the present study also appears suitable for extension to horizontal tail design under high-speed flight conditions, which represent another critical aspect of aircraft performance. Moreover, the optimized aero-shapes obtained in this work will serve as the basis for the development of a morphing architecture capable of reproducing the target geometries.

The research activities described in this paper were carried out within the framework of the European Union co-funded HERFUSE project (Hybrid-Electric Regional Fuselage & Empennages).

5 Acknowledgement

Authors acknowledge all HERFUSE Partners for their technical support and the European Union for co-funding the activities.

6 Funding

The activities described in this paper have been carried out within HERFUSE (Hybrid-Electric Regional FUSelage & Empennages) project; which has received funding from the European Union's Horizon Europe research and innovation programme under grant agreement No 101140567.

7 Disclaimer

Views and opinions expressed are however those of the author(s) only and do not necessarily reflect those of the European Union or of the granting authority. Neither the European Union nor the granting authority can be held responsible for them.

8 Nomenclature

2D	two-dimensional
ADAM	Adaptive Moment Estimation
BLI	Boundary Layer Ingestion
CAJU	Clean Aviation Joint Undertaking
CFD	Computational Fluid Dynamics
CIRA	Italian Aerospace Research Centre
CMA-ES	Covariance Matrix Adaptation Evolution Strategy
CO2	Carbon dioxide
COP	Conference of the Parties
CORSIA	Carbon Offsetting and Reduction Scheme for International Aviation
e.g.	exempli gratia
ETS	Emissions Trading System
EU	European Union
GA	Genetic Algorithm
h	Altitude
HERFUSE	Hybrid-Electric Regional FUSelage & Empennages
ICAO	International Civil Aviation Organization
ISA	International Standard Atmosphere
LTAG	Long-Term Aspirational Goal
M	Mach number
MAC	Mean Aerodynamic Chord
MDO	Multidisciplinary Design Optimization
NAG	Nesterov Accelerated Gradient
NDC	Nationally Determined Contributions
NOX	Nitrogen Oxides
RBF	Radial Basis Function
SAF	Sustainable Aviation Fuels
SoA	State of Art
UAV	Unmanned Aerial Vehicles
UNFCCC	United Nations Framework Convention on Climate Change

9 References

[1] UNFCCC, “History of the Convention,” United Nations Climate Change. [Online]. Available: https://unfccc.int/process/the-convention/history-of-the-convention#Essential-background (accessed Jun. 18, 2026).

[2] UNFCCC, “Conference of the Parties (COP),” United Nations Climate Change. [Online]. Available: https://unfccc.int/process/bodies/supreme-bodies/conference-of-the-parties-cop (accessed Jun. 18, 2026).

[3] UNFCCC, “The Kyoto Protocol,” United Nations Climate Change. [Online]. Available: https://unfccc.int/process-and-meetings/the-kyoto-protocol (accessed Jun. 18, 2026).

[4] UNFCCC, “The Paris Agreement,” United Nations Climate Change. [Online]. Available: https://unfccc.int/process-and-meetings/the-paris-agreement (accessed Jun. 18, 2026).

[5] ICAO, “Carbon Offsetting and Reduction Scheme for International Aviation (CORSIA),” International Civil Aviation Organization. [Online]. Available: https://www.icao.int/CORSIA (accessed Jun. 18, 2026).

[6] ICAO, “Long-term global aspirational goal (LTAG) for international aviation,” International Civil Aviation Organization. [Online]. Available: https://www.icao.int/environmental-protection/long-term-global-aspirational-goal-ltag-international-aviation (accessed Jun. 18, 2026).

[7] European Commission, “EU Emissions Trading System (EU ETS),” Climate Action. [Online]. Available: https://climate.ec.europa.eu/eu-action/eu-emissions-trading-system-eu-ets_en (accessed Jun. 18, 2026).

[8] European Commission, “European Green Deal,” Climate Action. [Online]. Available: https://climate.ec.europa.eu/eu-action/european-green-deal_en (accessed Jun. 18, 2026).

[9] Clean Aviation Joint Undertaking, “Clean Aviation,” Clean Aviation. [Online]. Available: https://clean-aviation.eu/ (accessed Jun. 18, 2026).

[10] M. R. Chiarelli *et al.*, “Numerical investigation of a morphing wing section controlled by piezoelectric patches,” *Actuators*, vol. 14, Art. no. 499, 2025, doi: 10.3390/act14100499.

[11] A. Chellangi, S. Santhanam, and G. S. Reddy, “Design of aircraft morphing wing using shape memory alloy as an actuator,” *AIP Conf. Proc.*, vol. 3259, Art. no. 070001, 2025, doi: 10.1063/5.0263964.

[12] N. Simiriotis, M. Fragiadakis, J. F. Rouchon, and M. Braza, “Shape control and design of aeronautical configurations using shape memory alloy actuators,” *Comput. Struct.*, vol. 244, Art. no. 106434, 2021, doi: 10.1016/j.compstruc.2020.106434.

[13] S. Barbarino, O. Bilgen, R. M. Ajaj, M. I. Friswell, and D. J. Inman, “A review of morphing aircraft,” *J. Intell. Mater. Syst. Struct.*, vol. 22, no. 9, pp. 823–877, Jun. 2011, doi: 10.1177/1045389X11414084.

[14] J. Zhu, J. Yang, W. Zhang, X. Gu, and H. Zhou, “Design and applications of morphing aircraft and their structures,” *Front. Mech. Eng.*, vol. 18, no. 3, Art. no. 34, 2023, doi: 10.1007/s11465-023-0750-6.

[15] Q.-F. Jiang, S.-S. Chen, H. Yang, Z.-G. Zhang, and Z.-H. Gao, “Unsteady aerodynamic characteristics of a morphing tail configuration,” *Phys. Fluids*, vol. 36, Art. no. 036133, 2024, doi: 10.1063/5.0199736.

[16] Clean Aviation Joint Undertaking, “Clean Sky’s morphing wing project brings shape-shifting capabilities to European regional aircraft,” Clean Aviation. [Online]. Available: https://www.clean-aviation.eu/research-and-innovation/clean-sky-2/results-stories/clean-skys-morphing-wing-project-brings-shape-shifting-capabilities-to-european-regional-aircraft (accessed Jun. 18, 2026).

[17] Clean Sky 2 Joint Undertaking, “Clean Sky 2 achievement report 2014–2024: A decade of innovation for a sustainable European aviation industry,” 2025.

[18] CompositesWorld, “Clean Aviation’s regional aircraft technology testbed 2 demonstrates advances with composites,” CompositesWorld. [Online]. Available: https://www.compositesworld.com/news/clean-aviations-regional-aircraft-technology-testbed-2-demonstrates-advances-with-composites (accessed Jun. 18, 2026).

[19] Clean Aviation Joint Undertaking, “Adaptive wing integrated demonstrator – flying test bed outer wing box,” Clean Aviation. [Online]. Available: https://www.clean-aviation.eu/research-and-innovation/clean-sky-2/clean-sky-2-achievement-report/clean-sky-2s-key-achievements/adaptive-wing-integrated-demonstrator-flying-test-bed-outer-wing-box (accessed Jun. 18, 2026).

[20] P. Della Vecchia, “READ_9,” Univ. Naples Federico II. [Online]. Available: http://wpage.unina.it/pierluigi.dellavecchia/pdf/publications/conferences/READ_9.pdf (accessed Jun. 18, 2026).

[21] D. Ciliberti, P. Della Vecchia, F. Nicolosi, and A. De Marco, “Aircraft directional stability and vertical tail design: A review of semi-empirical methods,” *Prog. Aerosp. Sci.*, vol. 95, pp. 140–172, 2017.

[22] F. Nicolosi and P. Della Vecchia, “Wind tunnel tests of innovative tailplane configurations,” in *Proc. 34th Congr. Int. Council Aeronaut. Sci. (ICAS)*, 2024, Paper 18.

[23] MIT OpenCourseWare, “16.333 Aircraft stability and control, Fall 2004: Lecture notes,” Massachusetts Inst. Technol. [Online]. Available: https://ocw.mit.edu/courses/16-333-aircraft-stability-and-control-fall-2004/pages/lecture-notes/ (accessed Jun. 18, 2026).

[24] J.-X. Leng, Z.-G. Wang, W. Huang, Y. Shen, and K. An, “Multidisciplinary design optimization processes for efficiency improvement of aircraft: State-of-the-art review,” *Int. J. Aeronaut. Space Sci.*, vol. 26, pp. 2020–2042, 2025, doi: 10.1007/s42405-024-00811-8.

[25] J. Nocedal and S. J. Wright, *Numerical Optimization*, 2nd ed. New York, NY, USA: Springer, 2006.

[26] F. Grasso, “Multi-objective numerical optimization applied to aircraft design,” Ph.D. dissertation, Univ. Naples Federico II, Naples, Italy, 2008, doi: 10.6092/UNINA/FEDOA/3188.

[27] M. Malavoti, “Mid-fidelity numerical approach to aerodynamic and aeroacoustic design of a Lift+Cruise eVTOL aircraft,” M.S. thesis, Aeronaut. Eng., Politecnico di Milano, Milan, Italy, 2025.

[28] P. D. Bravo-Mosquera, H. D. Cerón-Muñoz, and F. M. Catalano, “Design, aerodynamic analysis and optimization of a next-generation commercial airliner,” *J. Braz. Soc. Mech. Sci. Eng.*, vol. 44, Art. no. 609, 2022, doi: 10.1007/s40430-022-03924-x.

[29] “Aerodynamic numerical optimization in UAV design,” Special Issue, *Aerospace*, ISSN 2226-4310, Section Aeronautics.

[30] D. Quagliarella, “Aerodynamic shape design using evolutionary computation: A tutorial with examples and case studies,” in *Computational Intelligence in Aerospace Sciences*, M. Vasile and V. M. Becerra, Eds. Reston, VA, USA: AIAA, 2014, ch. 15, pp. 529–581.

[31] D. Quagliarella, P. Iannelli, P. L. Vitagliano, and G. Chinnici, “Aerodynamic shape design using hybrid evolutionary computation and fitness approximation,” in *Proc. 1st AIAA Intell. Syst. Tech. Conf.*, 2004.

[32] D. Quagliarella, “Value-at-risk and conditional value-at-risk in optimization under uncertainty,” in *Uncertainty Management for Robust Industrial Design in Aeronautics*, C. Hirsch, D. Wunsch, J. Szumbarski, Ł. Łaniewski-Wołłk, and J. Pons-Prats, Eds. Cham, Switzerland: Springer, 2018, doi: 10.1007/978-3-319-77767-2_34.

[33] E. Morales and D. Quagliarella, “Risk measures in the context of robust and reliability based optimization,” in *Optimization Under Uncertainty with Applications to Aerospace Engineering*, M. Vasile, Ed. Cham, Switzerland: Springer, 2021, doi: 10.1007/978-3-030-60166-9_13.

[34] N. Hansen and A. Ostermeier, “Completely derandomized self-adaptation in evolution strategies,” *Evol. Comput.*, vol. 9, no. 2, pp. 159–195, Jun. 2001, doi: 10.1162/106365601750190398.

[35] A. Iske, “Radial basis functions: Basics, advanced topics and meshfree methods for transport problems,” *Rend. Sem. Mat. Univ. Politec. Torino*, vol. 61, pp. 247–285, 2003.

[36] A. de Boer, M. S. van der Schoot, and H. Bijl, “Mesh deformation based on radial basis function interpolation,” *Comput. Struct.*, vol. 85, nos. 11–14, pp. 784–795, Jun. 2007, doi: 10.1016/j.compstruc.2007.01.013.

[37] S. Jakobsson and O. Amoignon, “Mesh deformation using radial basis functions for gradient-based aerodynamic shape optimization,” *Comput. Fluids*, vol. 36, pp. 1119–1136, 2007, doi: 10.1016/j.compfluid.2006.11.002.